Coherent Phonon Pairs and Rotational Symmetry Breaking of Charge Density Wave Order in the Kagome Superconductor CsV_3Sb_5

Qinwen Deng,[1] Hengxin Tan,[2] Brenden R. Ortiz,[3,4] Andrea Capa Salinas,[3] Stephen D. Wilson,[3] Binghai Yan,[2,5] and Liang Wu[1,*]

[1] *Department of Physics and Astronomy, University of Pennsylvania, Philadelphia, Pennsylvania 19104, U.S.A.*
[2] *Department of Condensed Matter Physics, Weizmann Institute of Science, Rehovot, Israel*
[3] *Materials Department, University of California Santa Barbara, Santa Barbara, California 93106, U.S.A.*
[4] *Materials Science and Technology Division, Oak Ridge National Laboratory, Oak Ridge, Tennessee 37831, U.S.A.*
[5] *Department of Physics, The Pennsylvania State University, University Park, Pennsylvania 16802, U.S.A.*

(Dated: September 16, 2025)

In this work, we perform ultrafast time-resolved reflectivity measurements to study the symmetry breaking in the charge-density wave (CDW) phase of CsV_3Sb_5. By extracting the coherent phonon spectrum in the CDW phase of CsV_3Sb_5, we discover close phonon pairs near 1.3 THz and 3.1 THz, as well as a new mode at 1.84 THz. The 1.3 THz phonon pair and the 1.84 THz mode are observed up to the CDW transition temperature. Combining density-functional theory calculations, we point out these phonon pairs arise from the coexistence of Star-of-David and inverse Star-of-David distortions combined with six-fold rotational symmetry breaking. An anisotropy in the magnitude of transient reflectivity change is also revealed at the onset of CDW order. Our results thus indicate broken six-fold rotational symmetry in the charge-density wave state of CsV_3Sb_5, along with the absence of nematic fluctuation above T_{CDW}. Meanwhile, the measured coherent phonon spectrum in the CDW phase of $CsV_3Sb_{5-x}Sn_x$ with x = 0.03-0.04 matches with staggered inverse Star-of-David with interlayer π phase shift. This CDW structure contrasts with undoped CsV_3Sb_5 and explains the evolution from phonon pair to a single mode at 1.3 THz by x = 0.03-0.04 Sn-doping.

The Kagome lattice, hosting a corner-sharing triangle network, has been the focus of extensive research for decades due to its interplay of inherent geometrical frustrations, nontrivial topology and unconventional correlation effects. As a recent example, the newly discovered vanadium-based Kagome superconductors AV_3Sb_5 (A = K, Rb or Cs) have attracted tremendous research interest due to their unconventional electronic landscape, including charge density wave (CDW) below $T_{CDW} \approx$ 78-102 K and superconductivity with $T_c \approx$ 0.9-2.5 K[1–4]. More intriguingly, additional exotic electronic instabilities emerge inside the CDW phase, including signatures of a possible time-reversal symmetry breaking loop current state[5–16], electronic nematicity[17–22], and pair density wave within the superconducting state[23]. Therefore, it is of paramount significance to clarify the structure and symmetry of the CDW order in this family of compounds, in order to understand the interaction between this plethora of charge orders and superconductivity.

An abundance of initial experiments reported a 3D CDW state in AV_3Sb_5[24–26]. Among all members in this family of materials, CsV_3Sb_5 possesses the largest variety of reported 3D CDW phases with different interlayer stacking orders. These 3D CDW orders can be constructed from unstable phonon modes at M and L points in the momentum space which give rise to various $2 \times 2 \times 2$ CDW patterns[27–31]. The in-plane 2×2 distortions on the Kagome lattice can be characterized by either a Star-of-David (SD) or inverse Star-of-David (ISD) pattern [10, 27, 29] (Fig. 1a, b), with a well-defined phasing of 0 or π between neighboring Kagome layers. The relative energy of different CDW structures is very close, and consensus has not been made on the precise ground state configuration despite extensive research. Different measurements mainly evidenced either the LLL phase with alternative SD + ISD without interlayer π phase shift [32–36] (Fig. 1d), in which the six-fold rotational symmetry C_6 is preserved, or the MLL phase with ISD + ISD with interlayer π phase shift[9, 37–41] (Fig. 1c), in which the six-fold rotational symmetry is broken down to two-fold. A further $2 \times 2 \times 4$ supercell was also reported to coexist and compete with the $2 \times 2 \times 2$ structures [39, 42, 43] as observed by X-ray diffraction, with contradicting results whether this $2 \times 2 \times 4$ phase only has C_2[26, 39, 42, 44]. This is possibly due to the phase coexistence, locally of multiple CDW ordered states as reported by recent dark-field X-ray results[45]. Apart from whether the system breaks six-fold rotational symmetry, another major debate is at what temperature the six-fold symmetry breaks. Various experimental probes produced conflicting results regarding the onset temperature of rotational symmetry breaking, either at T_{CDW}[9, 42, 46] or much lower than T_{CDW}[8, 17–19, 47] via a distinct electronic nematic state. Therefore, whether the two-fold symmetry is directly related to the CDW has not yet been made clear. Another important question is whether fluctuations of these exotic electronic states emerge above T_{CDW} in CsV_3Sb_5. Strong CDW fluctuations and nematic states have been reported above T_{CDW}[21, 48, 49], although recent strain dependent measurements showed no fluctuating vestigial nematicity[22].

* liangwu@sas.upenn.edu

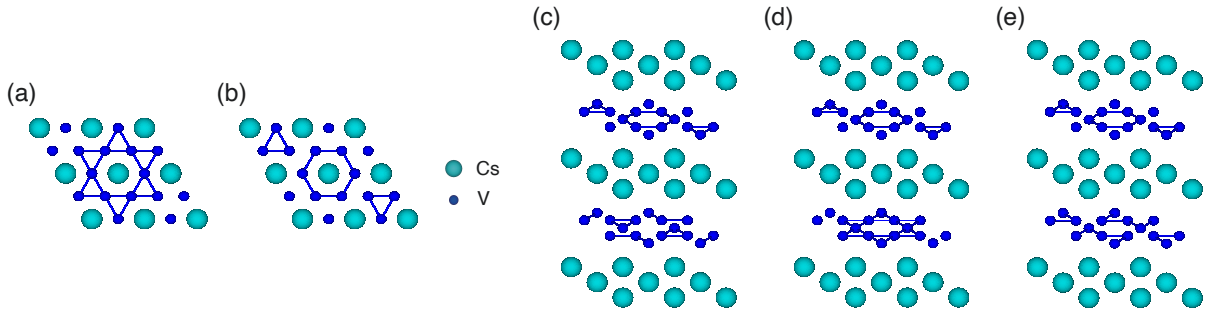

FIG. 1. **CDW distortions in CsV_3Sb_5.** (a) 2 × 2 × 1 SD. (b) 2 × 2 × 1 ISD. (c) ISD + ISD with interlayer π-phase shift, (d) SD + ISD without interlayer phase shift, and (e) SD + ISD with interlayer π-phase shift. The Cs atoms are shown in cyan and V atoms are shown in blue. The Sb atoms are not shown for simplicity. Note that only the structure in (a, b, d) keeps the D_{6h} symmetry. The lines connecting V atoms indicate shorter V-V bonds.

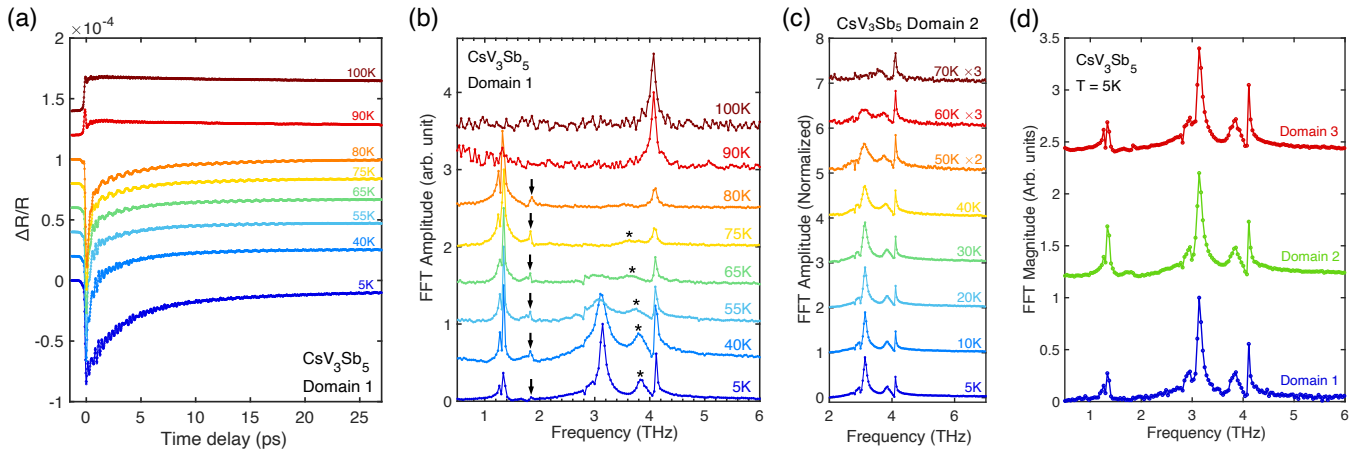

FIG. 2. **Temperature-dependent coherent phonon spectroscopy in Kagome CsV_3Sb_5.** (a) Time-resolved reflectivity curves at different temperatures above and below T_{CDW} in a single birefringence domain. (b) Amplitudes of Fourier transforms of coherent phonon oscillations in (a) after subtracting a double-exponential background. The arrow marks the temperature evolution of the 1.84 THz mode, and the asterisk marks the temperature evolution of the 3.86 THz mode. (c) Same as (b) but measured in another birefringence domain and zoomed in around 4 THz to better show the two close modes near 3.1 THz. All datasets are normalized to its maximum amplitude. (d) Coherent phonon spectrum measured on all 3 different birefringence domains at 5 K. Curves are offset for clarity in all plots.

In this work, we use ultrafast time-resolved reflectivity (TR-reflectivity) experiments to study the structural symmetry of the CDW phase of CsV_3Sb_5. The derived coherent phonon spectrum reveals close phonon pairs at 1.3 and 3.1 THz and a newly discovered mode at 1.84 THz. The 1.3 THz phonon pair and the 1.84 THz mode persist up to T_{CDW}. By comparing the calculated phonon frequencies using density functional theory (DFT), we demonstrate the close phonon pairs originate from the coexistence of SD and ISD pattern combined with six-fold rotational symmetry breaking. An anisotropy of the transient reflectivity change (ΔR/R), defined as non-equal ΔR/R values between two orthogonal polarization directions, also occurs upon entering CDW state. Our results thus unequivocally corroborate six-fold rotational symmetry breaking in the CDW phase of CsV_3Sb_5. Meanwhile, we pinpoint the CDW structure of $CsV_3Sb_{5-x}Sn_x$ with x = 0.03-0.04 to ISD + ISD with interlayer π-phase shift, which reduces the 1.3 THz phonon pair to a single phonon mode.

CsV_3Sb_5 single crystals are synthesized using the self-flux method[1, 3]. We perform TR-reflectivity measurements on freshly cleaved (001) surface of CsV_3Sb_5 single crystals. For all pump-probe experiments, pump wavelength is at 1560 nm and probe wavelength is at 780 nm, with repetition rate of 80 MHz and pulse duration of 100 fs. To reduce sample heating, both beams have a fluence less than 10 $\mu J/cm^2$. Both beams are at normal incidence and focused by an objective lens to achieve a spot size of ∼10 μm in diameter. In our previous experiments[9], we pinpointed the three-state birefringence domains in CsV_3Sb_5 below T_{CDW}, with the domain size being ∼100

μm. We can thus probe the transient reflectivity change in a single birefringence domain. Here, we use an xyz-stage to carefully adjust the light spot position onto a selected birefringence domain. The pump beam intensity is modulated at a frequency of 84 kHz using a photo-elastic modulator.

The coherent phonon generation via the pump pulse modulates the refractive index by the ion motion[50–52] which causes transient reflectivity changes. Fig. 2a shows the transient reflectivity change (ΔR/R) versus the pump-probe time delay measured inside a single birefringence domain of CsV_3Sb_5 at different temperatures. A single phonon oscillation can be observed above the CDW transition temperature T_{CDW} ~90 K. In contrast, the sign of the transient reflectivity traces flips below T_{CDW}, with the emergence of multiple phonon modes, as can be observed from the complex oscillation pattern. To better understand the evolution of coherent phonon modes as a function of temperature in the CDW phase, a double exponential decay background $(A_0+A_1\exp(-t/\tau_1)+A_2\exp(-t/\tau_2))$ is fitted to all time traces and then subtracted to show the oscillation parts, which are then Fourier transformed to reveal the coherent phonon modes (Fig. 2b). Above T_{CDW}, only one mode at 4.1 THz exists. This 4.1 THz mode persists at all temperatures and should be assigned as a main lattice mode. Indeed, it matches with a 4.10 THz A_{1g} mode in the pristine phase of CsV_3Sb_5 (Table I). In contrast, at T = 5 K, another two intense modes centered at 1.3 and 3.1 THz are conspicuously present, similar to previous pump-probe reflectivity studies[38, 53]. As temperature increases, the 1.3 THz mode exhibits an increase in amplitude but an abrupt disappearance at T $\approx$ 90 K, matching with reported T_{CDW} = 94 K[2, 54]. We note modest local laser heating may cause a slight decrease of the measured T_{CDW}. Little frequency softening is seen for the 1.3 THz mode when increasing the temperature, more consistent with a zone-folded phonon mode by CDW[55]. This explains its disappearance in the phonon spectrum above T_{CDW}. In contrast, the amplitude of 3.1 THz mode decreases during warm-up and vanishes at ~65 K (Fig. 2b, c). Same behavior is also captured in previous calculations[43]. Previous Raman studies [56, 57] showed this 3.1 THz mode exhibits significant weakening and broadening upon warming toward T_{CDW}, becoming overdamped between 60 and 90 K with the linewidth as large as 50 cm^{-1} right below T_{CDW}. This may explain why this 3.1 THz mode vanishes in our detection above ~65 K. Apart from these dominant modes, we also find a 3.86 THz mode and a weaker 1.84 THz mode that is newly-discovered by time-resolved reflectivity (Fig. 2b). Similar to the 1.3 THz mode, the 1.84 THz mode also shows little frequency change and persists up to T_{CDW}. We do not observe other modes up to 15 THz.

Contrary to previously reported pump-probe experiments on CsV_3Sb_5[38, 46, 53], we observe clear close phonon pairs near both 1.3 THz and 3.1 THz in our phonon spectrum. At T = 5 K, the 1.3 THz mode consists of two close phonon modes as shown in Fig. 2b with two peaks centered at 1.26 THz and 1.33 THz, respectively. These dual modes persists upon warming, up to T_{CDW} where it vanishes. Additionally, two close phonon peaks correspond to beatings in the time domain. Indeed, the beating waveform arising from these dual modes near 1.3 THz can be resolved in longer time scans (Fig. 3) with delay time difference of ~14 ps between wave nodes, in accordance with the frequency splitting (~ 0.07 THz) between these two peaks. Repeated measurements on another CsV_3Sb_5 sample also shows this 1.3 THz dual modes (Fig. 4). Meanwhile, same experiments on a second birefringence domain (Fig. 2c and Domain 2 in Fig. 2d) visualizes two close phonon modes near 3.1 THz, with

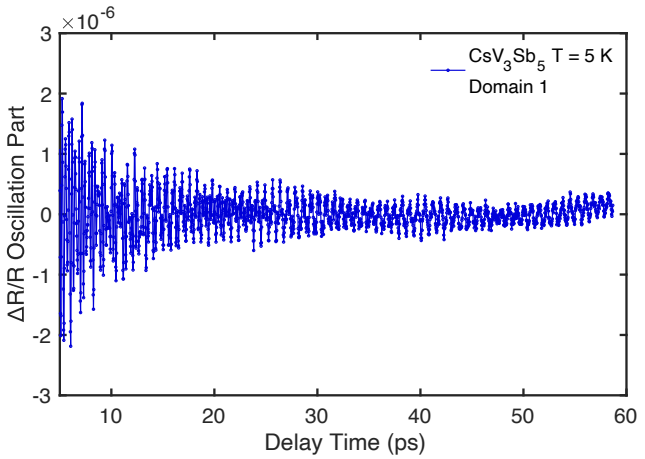

FIG. 3. Oscillation part of the TR-reflectivity curve corresponding to the phonon spectrum of domain 1 in Fig. 2. Clear beatings can be observed in the oscillation pattern which corroborates the dual modes near 1.3 THz. The data is taken at T = 5 K.

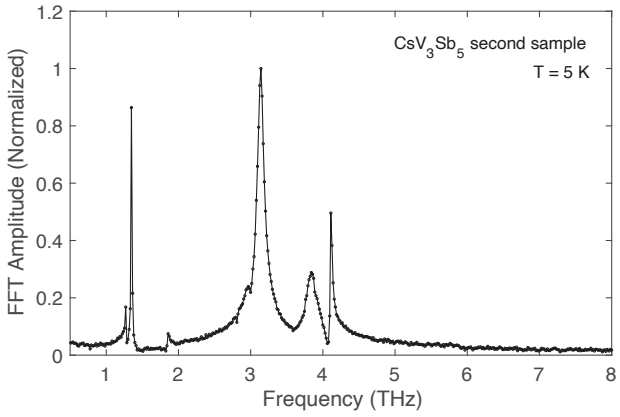

FIG. 4. Coherent phonon spectrum measured by TR-reflectivity on a second CsV_3Sb_5 sample at T = 5 K. It also shows the dual modes at 1.3 THz and 3.1 THz, as well as the newly discovered weaker mode near 1.8 THz.

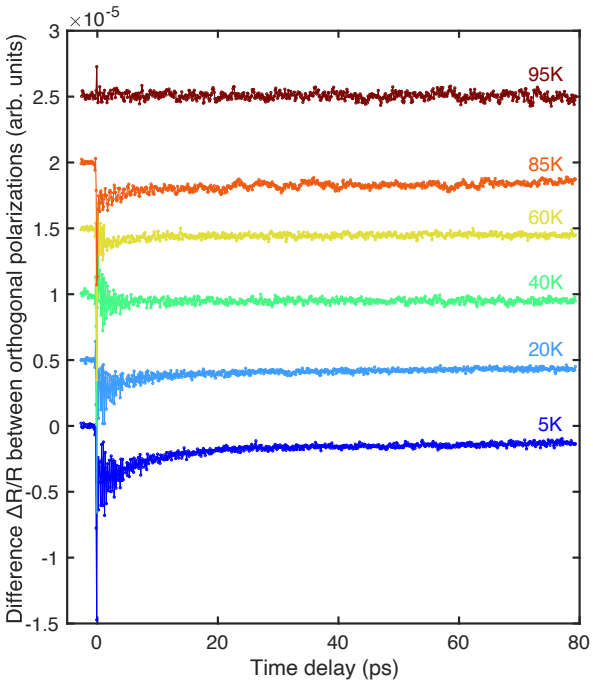

FIG. 5. Differential time-resolved reflectivity curves between orthogonal incident probe polarizations at different temperatures across T_{CDW}. The curves are offset for clarity. The light spot position is inside a single birefringence domain. Nonzero differential values below T_{CDW} indicates in-plane anisotropy, suggesting C_6 is broken. However, no difference is observed beyond noise level above T_{CDW}, indicating the preserve of C_6 and absence of nematic fluctuations.

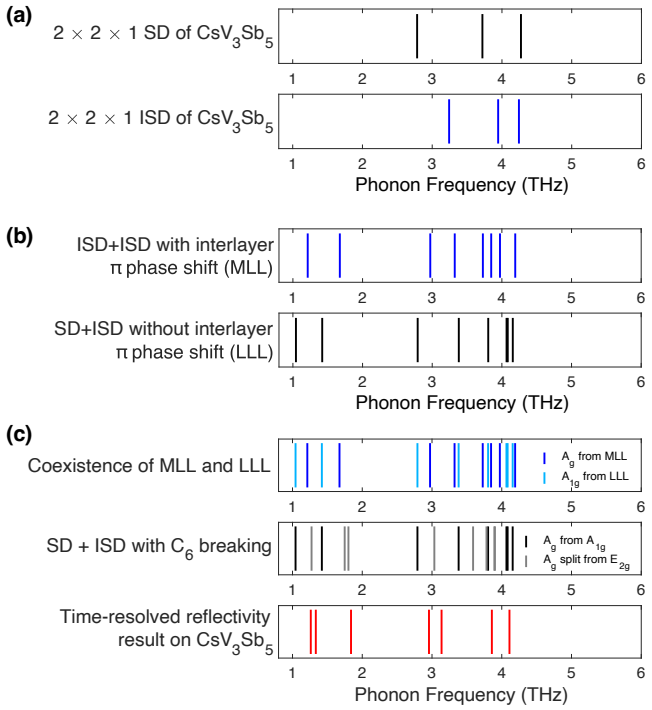

FIG. 6. **Comparison of the DFT results and the measured phonon modes by TR-reflectivity on CsV_3Sb_5 at T = 5 K.** The vertical lines denote the frequency of the $A_{1g}(A_g)$ modes in DFT calculation results or the measured phonon frequency. For DFT-calculated phonons, only the modes below 4.5 THz are shown. (a) The calculated A_{1g} mode frequencies in SD and ISD CDW phases in CsV_3Sb_5. (b) The calculated A_g (A_{1g}) mode frequencies in the ISD + ISD with interlayer π phase shift (SD + ISD without interlayer π phase shift) CDW order. (c) The calculated fully-symmetric mode frequencies in the CDW order with the coexistence of MLL and LLL, and the calculated A_g mode frequencies in SD + ISD with C_6 breaking CDW phases in CsV_3Sb_5 and their comparison to the observed phonon modes in our TR-reflectivity results.

its two peaks centered at 2.96 THz and 3.14 THz at T = 5 K. These two close modes persist up to 60 K when the 3.1 THz mode fades away in our detection. Moreover, both 1.3 and 3.1 THz phonon pairs are visible in the coherent phonon spectrum extracted from all three birefringence domains (Fig. 2d).

Furthermore, we reveal evidence of C_6 breaking from the anisotropy of transient reflectivity response by varying probe polarizations, which manifests breaking of rotational symmetry and has been used to study the nematic order in Fe-based superconductors[58–60]. This probe polarization dependent measurement has also been successfully used to probe the breaking of C_6 in Kagome CDW material $CsCr_3Sb_5$[61]. By varying the probe polarization within the (001) surface, we observe the anisotropic transient reflectivity signal inside the Kagome plane at T = 5 K, indicating broken C_6. To highlight this anisotropy, we subtract the signals from orthogonal probe polarization states that correspond to maximum and minimum signal size respectively. As shown in Fig. 5, this anisotropy persists in the CDW phase but vanishes above T_{CDW}, corroborating C_6 breaking onsets at the CDW transition. Further probe polarization dependent measurements are shown in Appendix B. This is different from the low-temperature electronic nematic order seen by NMR[17] and STM quasiparticle interference measurement[18, 47] that onsets at $\sim$ 35 K far below T_{CDW}. Our observed isotropic response of transient reflectivity above T_{CDW} demonstrates C_6 symmetry, sharing the conclusion of Liu et al.[22] suggesting no vestigial nematic order associated with the C_6-breaking CDW.

To explain the observed close phonon modes and determine the CDW structure of CsV_3Sb_5, we perform DFT calculations of phonon frequencies and compare with the phonon spectrum detected by TR-reflectivity. In TR-reflectivity measurements, the femtosecond pump pulse selectively excites Raman-active phonons coherently[62, 63]. On the theory side, coherent phonon excitation is often described either as impulsive stimulated Raman scattering (ISRS)[64–66] or as displacive excitation of coherent phonons (DECP)[67, 68]. In ISRS, there is no restrictions on the symmetry of the Raman-active modes[64], and ISRS does not require absorption in the

Pristine	A_{1g}	E_{2g}							
	4.10	3.86							
$2 \times 2 \times 1$ SD	A_{1g}	A_{1g}	A_{1g}	E_{2g}	E_{2g}	E_{2g}	E_{2g}		
	2.78	3.72	4.27	1.49	1.65	3.58	3.88		
$2 \times 2 \times 1$ ISD	A_{1g}	A_{1g}	A_{1g}	E_{2g}	E_{2g}	E_{2g}	E_{2g}		
	3.24	3.95	4.24	1.73	2.97	3.74	3.87		
ISD + ISD with interlayer π phase shift	A_g	A_g	A_g	A_g	A_g	A_g	A_g	A_g	
	1.21	1.67	2.97	3.32	3.73	3.85	3.97	4.19	
SD + ISD without interlayer π phase shift	A_{1g}	A_{1g}	A_{1g}	A_{1g}	A_{1g}	A_{1g}	A_{1g}	A_{1g}	
	1.04	1.42	2.79	3.38	3.80	4.07	4.08	4.16	
	E_{2g}	E_{2g}	E_{2g}	E_{2g}	E_{2g}	E_{2g}	E_{2g}	E_{2g}	E_{2g}
	0.31	1.27	1.75	1.80	3.03	3.59	3.78	3.89	3.90

TABLE I. Frequency (unit: THz) of the selected Raman-active modes in the pristine and CDW phases of CsV_3Sb_5 calculated by DFT. Only relevant A_{1g}, E_{2g} and A_g modes with frequencies below 4.5 THz are included. When interlayer π phase shift between the SD and ISD layer is included, the E_{2g} modes in the SD + ISD without interlayer π phase shift (LLL) phase will split to induce A_g modes that can be detected in TR-reflectivity.

material[69, 70]. Meanwhile, DECP requires absorption at the pump frequency in order to disturb the electronic energy distribution in the material, and only fully symmetric modes can be observed[67, 68] in DECP mechanism. Fully symmetric phonon modes host Γ_1^+ symmetry, such as A_{1g} modes in D_{6h} point group and A_g modes in D_{2h} point group.

To determine the coherent phonon excitation mechanism in our pump-probe measurement, we first compare our detected phonon modes with previous Raman spectroscopy results on CsV_3Sb_5[56, 71]. Above T_{CDW}, Raman spectroscopy detected one A_{1g} mode at 4.1 THz and one E_{2g} mode at 3.6 THz with comparable amplitudes. This main 3.6 THz E_{2g} mode persists across T_{CDW} at all temperatures and has the maximum amplitude among all non-fully-symmetric Raman-active modes, with minimal frequency change of less than 1 cm^{-1} ($\rightarrow$ 0.030 THz) and increasing amplitude as temperature increases[56, 71]. However, in our TR-reflectivity measurements, we only detect the 4.1 THz A_{1g} mode above T_{CDW}. Below T_{CDW}, we do not observe this strongest 3.6 THz E_{2g} mode either. The closest detected mode is the 3.86 THz mode, but it quickly weakens and softens as temperature increases, in contrast to the 3.6 THz E_{2g} mode. Since we do not observe this dominant 3.6 THz mode at any temperature, we can rule out the detection of non-fully-symmetric modes in our TR-reflectivity measurements. Meanwhile, our pump photon energy ($\sim$ 0.79 eV) is much larger than the partial CDW gap opening in CsV_3Sb_5[36, 72–74] indicating strong absorption at pump frequency. Further confirmation of DECP mechanism is shown in pump polarization dependent measurements detailed in Appendix C. We confirm therein the observed coherent phonons in the CDW state are all fully symmetric. Thus, we use the DECP mechanism to interpret our data, and we assume all the detected phonon modes in our time-resolved reflectivity measurements are fully symmetric modes. This also matches with previous pump-probe studies on CsV_3Sb_5[38].

We first examine the phonon spectra of the two C_6-symmetric $2 \times 2 \times 1$ CDW orders, SD and ISD, to see if they match with our observed phonon spectrum. Fig. 6a shows the DFT calculated A_{1g} phonon spectrum of SD and ISD phases in the relevant frequency region. Both phases lack the observed 1.3 and 3.1 THz phonon pairs and the 1.84 THz mode from our TR-reflectivity measurements.

Thus, we need to consider a modulation along c axis of the CDW order, which is consistent with previous X-ray diffraction studies[25, 42]. We first examine the two most reported $2 \times 2 \times 2$ CDW states (Fig. 6b): either ISD + ISD with interlayer π phase shift (MLL), where the C_6 rotational symmetry is broken, or SD + ISD without interlayer π phase shift (LLL), where C_6 is preserved. The calculated fully-symmetric A_g (A_{1g}) mode frequencies in the ISD + ISD with interlayer π phase shift (SD + ISD without interlayer π phase shift) CDW order has been listed in Table I and plotted in Fig. 6b. The MLL phase agrees with our TR-reflectivity results better, with the frequency difference of the two A_g modes near 3.1 THz closer to the observed value. The MLL phase also hosts an A_g mode at 1.67 THz that matches the observed 1.84 THz phonon. This A_g mode comes from the C_6-breaking induced split of an E_{2g} mode at 1.73 THz in $2 \times 2 \times 1$ ISD phase (Table I) ($E_{2g} \rightarrow A_g + B_{1g}$). However, MLL only shows one A_g mode near 1.3 THz, which fails to explain the observed two close modes near 1.3 THz. For the LLL phase, although it has two A_{1g} phonon pairs near 1.3 THz and 3.1 THz, their frequency differences are too large to match the measured values of our observed 1.3 THz and 3.1 THz phonon pairs. Also, no A_{1g} mode in LLL matches well with our observed 1.84 THz mode. Fi-

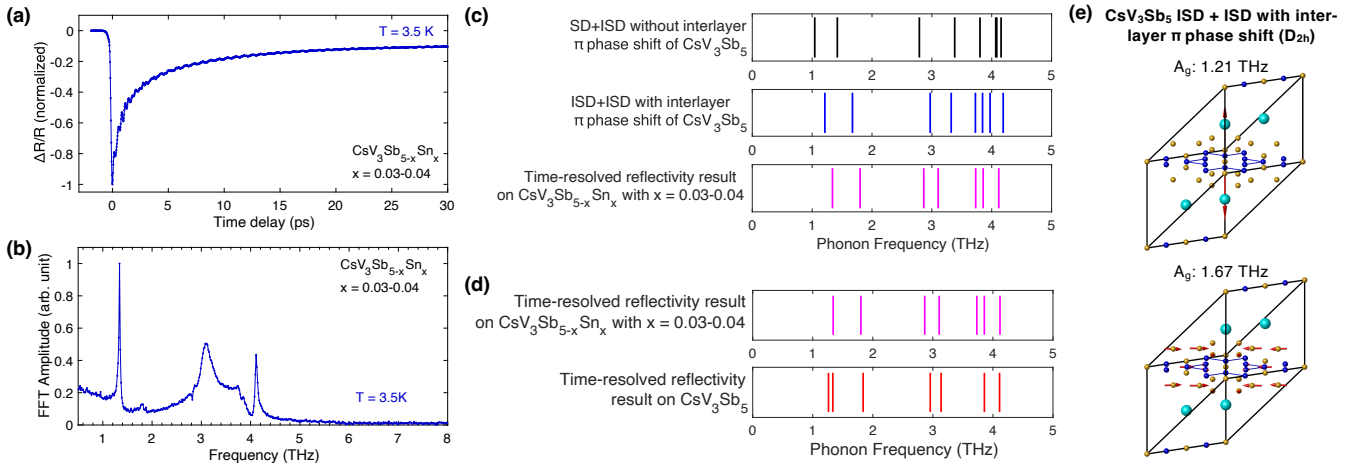

FIG. 7. **Coherent phonon spectrum in $CsV_3Sb_{5-x}Sn_x$ with x = 0.03-0.04.** (a) TR-reflectivity time trace on $CsV_3Sb_{5-x}Sn_x$ with x = 0.03-0.04 at T = 3.5 K. (b) Coherent phonon spectrum measured from TR-reflectivity at T = 3.5 K. (c) The calculated A_{1g} (A_g) mode frequencies in the SD + ISD without interlayer π phase shift (ISD + ISD with interlayer π phase shift) CDW state in CsV_3Sb_5 and their comparison to our TR-reflectivity results in $CsV_3Sb_{5-x}Sn_x$ with x = 0.03-0.04. (d) Comparison of the measured coherent phonon spectrum by time-resolved reflectivity in CsV_3Sb_5 and $CsV_3Sb_{5-x}Sn_x$ with x = 0.03-0.04. In (c-d), The phonon spectrum of $CsV_3Sb_{5-x}Sn_x$ with x = 0.03-0.04 measured from TR-reflectivity is taken at T = 3.5 K. In (d), the phonon spectrum for CsV_3Sb_5 is taken at T = 5 K. (e) The DFT-calculated oscillation pattern of the fully-symmetric Raman active A_g modes in ISD + ISD with interlayer π phase shift (MLL) CDW state in CsV_3Sb_5 that are near our detected 1.34 and 1.80 THz modes in $CsV_3Sb_{5-x}Sn_x$ with x = 0.03-0.04 via time-resolved reflectivity, respectively. The 1.21 and 1.67 THz A_g modes are the lowest and second-lowest frequency mode in the A_g phonon spectrum of MLL phase in (c).

nally, our previous birefringence measurement indicates C_6 symmetry breaking[9], contradictory to the preserved C_6 in LLL. In short, either MLL or LLL cannot explain our observed coherent phonon spectrum in CsV_3Sb_5.

We note a recent time-resolved X-ray diffraction (XRD) measurement that demonstrated the coexistence of MLL and LLL CDW orders[75] which breaks C_6. By comparing the combined phonon spectrum of these two CDW orders, we point out this coexistence configuration can explain our experimentally detected phonon spectrum (Fig. 6c) by showing fully-symmetric phonon pairs near 1.3 and 3.1 THz and a fully-symmetric mode near 1.8 THz, explaining our measured phonon spectrum better than merely MLL or LLL. This coexistence of MLL and LLL phase will also be energetically favorable as it contains the reported two energetically favorable CDW phases MLL and LLL[27, 29]. Further evidence of the coexistence of MLL and LLL CDW orders comes from our pump fluence dependent TR-reflectivity measurements, as shown in Appendix D. Herein, we pinpoint the lower and higher frequency peak of the 1.3 THz dual modes originates from LLL and MLL phase respectively. The observed 1.84 THz phonon is then explained by the 1.67 THz A_g mode in MLL phase, which comes from C_6-breaking induced split of an E_{2g} mode at 1.73 THz in 2 × 2 × 1 ISD phase (Table I). While there are more fully-symmetric modes in calculation than observed, some modes could be missing in our observation, possibly due to their weaker modulations on the refractive index. Moreover, some calculated modes between 3.5 - 4 THz may be too close in frequency to be resolved individually in the measurements.

Besides, if C_6 is broken by interlayer π phase shift between the SD and ISD layer (Fig. 1e), E_{2g} modes in the C_6-symmetric LLL phase will split to give rise to a fully symmetric A_g mode that can be detected in TR-reflectivity. A_{1g} modes in LLL will also evolve into A_g modes. We list the A_g modes in this C_6-breaking SD + ISD state in Fig. 6c. In this phase, there also exists close 1.3 THz and 3.1 THz A_g pairs, along with A_g modes near 1.8 THz that are split from E_{2g} modes, i.e. the 1.75 and 1.80 THz E_{2g} mode in LLL (Table I). However, this SD + ISD with interlayer π-phase shift phase may not be among the most energetically stable phases[27, 29, 38]. Considering our pump fluence dependence data, recent time-resolved XRD results[75] and energy stability of these phases, the coexistence of MLL and LLL phase is more likely, but we can't fully rule out SD + ISD with interlayer π-phase shift.

In either case, our observed two close phonon pairs near 1.3 and 3.1 THz strongly corroborate C_6-breaking in the CDW phase of CsV_3Sb_5 and the coexistence of SD and ISD patterns. Meanwhile, to explain our observed 1.84 THz mode, C_6-breaking is also required to give rise to a fully symmetric A_g mode near 1.8 THz by splitting the corresponding E_{2g} mode. Thus, the persistence of two close modes near 1.3 THz and the 1.84 THz mode up to T_{CDW} in our measurements marks the C_6 breaking

happens simultaneously with the onset of CDW, contrary to the electronic nematicity revealed by NMR[17] and STM[18, 47] that only onset at temperatures far below T_{CDW}.

There is also a recent Raman measurement reporting two close modes near 1.3 THz[41] but only above $\sim$ 65 K. The temperature-dependent evolution of the intensities of these two modes indicated a spectral transformation between them and the higher frequency mode became weaker above $\sim$ 65 K. This is different from our TR-reflectivity results where the two close modes near 1.3 THz are always present from T_{CDW} down to 5 K, and our measured intensity of the higher frequency mode keeps increasing from 5 K to 80 K. We also note that an alternative interpretation based on calculation analysis has been proposed in [43], showing a 2 × 2 × 4 ISD-stacking phase coexisting with MLL provides a 1.4 THz mode which can combine with the 1.21 THz A_g mode in MLL to explain the observed dual 1.3 THz modes.

In contrast to pure CsV_3Sb_5, the investigation of TR-reflectivity on $CsV_3Sb_{5-x}Sn_x$ with x = 0.03-0.04 uncovers a different CDW structural reconstruction from CsV_3Sb_5. Fig. 7b shows the coherent phonon spectrum extracted from $\Delta R/R$ vs. time delay (Fig. 7a) in this x = 0.03-0.04 Sn-doped sample. Similar to CsV_3Sb_5, at T = 3.5 K, the most prominent modes are at 1.34, 3.11 and 4.18 THz, along with weaker peaks around 1.80 and 3.8 THz. However, in contrast to dual modes at 1.3 THz in CsV_3Sb_5, we observe only one mode at 1.34 THz in this Sn-doped sample, with its frequency matching the higher frequency peak in the 1.3 THz dual mode in undoped CsV_3Sb_5 (Fig. 7d). Meanwhile, the 3.11 THz mode is weaker and broader compared to CsV_3Sb_5, making its dual mode feature weaker. We then compare our detected phonon modes with the DFT-calculated fully-symmetric phonon spectrum in various CDW phases (Fig. 7c). Overall, the phonon spectrum of ISD + ISD with interlayer π-phase shift matches the experimental results better, since the observed 1.34, 1.80 and 3.11 THz modes are better matched in frequency. We thus conclude the actual CDW structure of this x = 0.03-0.04 sample to be ISD + ISD with interlayer π-phase shift (MLL), breaking C_6 rotational symmetry as well. This matches with recent ARPES[32] and X-ray diffraction[76] results. Thus, our observed 1.34 THz mode corresponds to the calculated 1.21 THz A_g mode which is a Cs-related mode, and our observed 1.80 THz mode corresponds to the calculated 1.67 THz A_g mode which involves V and Sb oscillations (Fig. 7e). The CDW structure in this x = 0.03-0.04 sample contrasts with the coexistence of SD and ISD distortion in undoped CsV_3Sb_5, which explains the evolution from dual modes to single mode at 1.3 THz by a slight x = 0.03-0.04 Sn-doping. The frequency match between the 1.34 THz mode in this x = 0.03-0.04 Sn-doped sample and the higher frequency peak in the 1.3 THz dual modes in undoped CsV_3Sb_5 indicates this higher frequency peak in the 1.3 THz dual modes in undoped CsV_3Sb_5 comes from MLL, matching with the conclusion in Appendix D and further confirms the coexistence of MLL and LLL CDW phase in undoped CsV_3Sb_5.

In conclusion, we have studied coherent phonon excitation in CsV_3Sb_5 via time-resolved reflectivity to determine the structural configuration of its CDW phase. The phonon spectra confirm six-fold rotational symmetry breaking and the coexistence of SD and ISD distortion in the CDW phase of CsV_3Sb_5. From our measurements and DFT calculations, there are two possibilities: coexistence of MLL and LLL, and SD + ISD with interlayer π-phase shift. Considering our fluence dependence measurements, we think coexistence of MLL and LLL phase is more likely, but we can't fully rule out SD + ISD with interlayer π-phase shift. Meanwhile, an x = 0.03-0.04 Sn-doping changes the CDW structure to MLL with only in-plane ISD distortion, reducing 1.3 THz dual modes in undoped CsV_3Sb_5 to a single mode. This observation provides deeper insights for comprehending the interplay with other electronic phases in this system, such as the in-plane 1 × 4 unidirectional charge order[18, 47, 77], electronic nematicity, and superconductivity. We also envision our methodology will promote the understanding of the CDW phase diagram in doped AV_3Sb_5[76, 78, 79] and other Kagome systems such as FeGe[80, 81], and stimulate further research on ultrafast manipulation of these symmetry-breaking states.

ACKNOWLEDGEMENT

The construction of the pump-probe setup was supported by the Air Force Office of Scientific Research under award no. FA9550-22-1-0410. Q.D. was mainly supported by the Vagelos Institute of Energy Science and Technology graduate fellowship and also partly supported by the Air Force Office of Scientific Research under award no. FA9550-22-1-0410 and the National Science Foundation EPM program under grant no. DMR-2213891. S.D.W. and B.R.O. gratefully acknowledge support via the UC Santa Barbara National Science Foundation Quantum Foundry funded via the Q-AMASE-i program under award DMR-1906325. B.R.O. thanks support from the U.S. Department of Energy (DOE), Office of Science, Basic Energy Sciences (BES), Materials Sciences and Engineering Division. B.Y. acknowledges the financial support by the Israel Science Foundation (ISF: 2932/21, 2974/23), German Research Foundation (DFG, CRC-183, A02), and by a research grant from the Estate of Gerald Alexander. L.W. acknowledges support from the Sloan Foundation under the award FG-2025-25036.

[1] B. R. Ortiz, L. C. Gomes, J. R. Morey, M. Winiarski, M. Bordelon, J. S. Mangum, I. W. Oswald, J. A. Rodriguez-Rivera, J. R. Neilson, S. D. Wilson, et al., New kagome prototype materials: discovery of kv 3 sb 5, rbv 3 sb 5, and csv 3 sb 5, Physical Review Materials **3**, 094407 (2019).

[2] B. R. Ortiz, S. M. Teicher, Y. Hu, J. L. Zuo, P. M. Sarte, E. C. Schueller, A. M. Abeykoon, M. J. Krogstad, S. Rosenkranz, R. Osborn, et al., Cs v 3 sb 5: A z 2 topological kagome metal with a superconducting ground state, Physical Review Letters **125**, 247002 (2020).

[3] B. R. Ortiz, P. M. Sarte, E. M. Kenney, M. J. Graf, S. M. Teicher, R. Seshadri, and S. D. Wilson, Superconductivity in the z 2 kagome metal kv 3 sb 5, Physical Review Materials **5**, 034801 (2021).

[4] Q. Yin, Z. Tu, C. Gong, Y. Fu, S. Yan, and H. Lei, Superconductivity and normal-state properties of kagome metal rbv3sb5 single crystals, Chinese Physics Letters **38**, 037403 (2021).

[5] C. Mielke III, D. Das, J.-X. Yin, H. Liu, R. Gupta, Y.-X. Jiang, M. Medarde, X. Wu, H. C. Lei, J. Chang, et al., Time-reversal symmetry-breaking charge order in a kagome superconductor, Nature **602**, 245 (2022).

[6] Y.-X. Jiang, J.-X. Yin, M. M. Denner, N. Shumiya, B. R. Ortiz, G. Xu, Z. Guguchia, J. He, M. S. Hossain, X. Liu, et al., Unconventional chiral charge order in kagome superconductor kv3sb5, Nature materials **20**, 1353 (2021).

[7] Y. Xing, S. Bae, E. Ritz, F. Yang, T. Birol, A. N. Capa Salinas, B. R. Ortiz, S. D. Wilson, Z. Wang, R. M. Fernandes, et al., Optical manipulation of the charge-density-wave state in rbv3sb5, Nature **631**, 60 (2024).

[8] C. Guo, C. Putzke, S. Konyzheva, X. Huang, M. Gutierrez-Amigo, I. Errea, D. Chen, M. G. Vergniory, C. Felser, M. H. Fischer, et al., Switchable chiral transport in charge-ordered kagome metal csv3sb5, Nature **611**, 461 (2022).

[9] Y. Xu, Z. Ni, Y. Liu, B. R. Ortiz, Q. Deng, S. D. Wilson, B. Yan, L. Balents, and L. Wu, Three-state nematicity and magneto-optical kerr effect in the charge density waves in kagome superconductors, Nature physics **18**, 1470 (2022).

[10] T. Park, M. Ye, and L. Balents, Electronic instabilities of kagome metals: saddle points and landau theory, Physical Review B **104**, 035142 (2021).

[11] X. Feng, K. Jiang, Z. Wang, and J. Hu, Chiral flux phase in the kagome superconductor av3sb5, Science bulletin **66**, 1384 (2021).

[12] M. M. Denner, R. Thomale, and T. Neupert, Analysis of charge order in the kagome metal a v 3 sb 5 (a= k, rb, cs), Physical Review Letters **127**, 217601 (2021).

[13] Y.-P. Lin and R. M. Nandkishore, Complex charge density waves at van hove singularity on hexagonal lattices: Haldane-model phase diagram and potential realization in the kagome metals a v 3 sb 5 (a= k, rb, cs), Physical Review B **104**, 045122 (2021).

[14] C. Guo, G. Wagner, C. Putzke, D. Chen, K. Wang, L. Zhang, M. Gutierrez-Amigo, I. Errea, M. G. Vergniory, C. Felser, et al., Correlated order at the tipping point in the kagome metal csv3sb5, Nature Physics **20**, 579 (2024).

[15] M. H. Christensen, T. Birol, B. M. Andersen, and R. M. Fernandes, Loop currents in a v 3 sb 5 kagome metals: Multipolar and toroidal magnetic orders, Physical Review B **106**, 144504 (2022).

[16] R. Tazai, Y. Yamakawa, and H. Kontani, Drastic magnetic-field-induced chiral current order and emergent current-bond-field interplay in kagome metals, Proceedings of the National Academy of Sciences **121**, e2303476121 (2024).

[17] L. Nie, K. Sun, W. Ma, D. Song, L. Zheng, Z. Liang, P. Wu, F. Yu, J. Li, M. Shan, et al., Charge-density-wave-driven electronic nematicity in a kagome superconductor, Nature **604**, 59 (2022).

[18] H. Li, H. Zhao, B. R. Ortiz, Y. Oey, Z. Wang, S. D. Wilson, and I. Zeljkovic, Unidirectional coherent quasiparticles in the high-temperature rotational symmetry broken phase of a v3sb5 kagome superconductors, Nature Physics **19**, 637 (2023).

[19] Y. Xiang, Q. Li, Y. Li, W. Xie, H. Yang, Z. Wang, Y. Yao, and H.-H. Wen, Twofold symmetry of c-axis resistivity in topological kagome superconductor csv3sb5 with in-plane rotating magnetic field, Nature communications **12**, 6727 (2021).

[20] D. Wulferding, S. Lee, Y. Choi, Q. Yin, Z. Tu, C. Gong, H. Lei, S. Yousuf, J. Song, H. Lee, et al., Emergent nematicity and intrinsic versus extrinsic electronic scattering processes in the kagome metal csv 3 sb 5, Physical Review Research **4**, 023215 (2022).

[21] T. Asaba, A. Onishi, Y. Kageyama, T. Kiyosue, K. Ohtsuka, S. Suetsugu, Y. Kohsaka, T. Gaggl, Y. Kasahara, H. Murayama, et al., Evidence for an odd-parity nematic phase above the charge-density-wave transition in a kagome metal, Nature Physics **20**, 40 (2024).

[22] Z. Liu, Y. Shi, Q. Jiang, E. W. Rosenberg, J. M. DeStefano, J. Liu, C. Hu, Y. Zhao, Z. Wang, Y. Yao, et al., Absence of e 2 g nematic instability and dominant a 1 g response in the kagome metal csv 3 sb 5, Physical Review X **14**, 031015 (2024).

[23] H. Chen, H. Yang, B. Hu, Z. Zhao, J. Yuan, Y. Xing, G. Qian, Z. Huang, G. Li, Y. Ye, et al., Roton pair density wave in a strong-coupling kagome superconductor, Nature **599**, 222 (2021).

[24] Z. Liang, X. Hou, F. Zhang, W. Ma, P. Wu, Z. Zhang, F. Yu, J.-J. Ying, K. Jiang, L. Shan, et al., Three-dimensional charge density wave and surface-dependent vortex-core states in a kagome superconductor csv 3 sb 5, Physical Review X **11**, 031026 (2021).

[25] H. Li, T. Zhang, T. Yilmaz, Y. Pai, C. Marvinney, A. Said, Q. Yin, C. Gong, Z. Tu, E. Vescovo, et al., Observation of unconventional charge density wave without acoustic phonon anomaly in kagome superconductors a v 3 sb 5 (a= rb, cs), Physical Review X **11**, 031050 (2021).

[26] B. R. Ortiz, S. M. Teicher, L. Kautzsch, P. M. Sarte, N. Ratcliff, J. Harter, J. P. Ruff, R. Seshadri, and S. D. Wilson, Fermi surface mapping and the nature of charge-density-wave order in the kagome superconductor csv 3 sb 5, Physical Review X **11**, 041030 (2021).

[27] M. H. Christensen, T. Birol, B. M. Andersen, and R. M. Fernandes, Theory of the charge density wave in a v 3 sb 5 kagome metals, Physical Review B **104**, 214513 (2021).

[28] E. T. Ritz, R. M. Fernandes, and T. Birol, Impact of sb degrees of freedom on the charge density wave phase diagram of the kagome metal csv 3 sb 5, Physical Review B **107**, 205131 (2023).

[29] H. Tan, Y. Liu, Z. Wang, and B. Yan, Charge density waves and electronic properties of superconducting kagome metals, Physical review letters **127**, 046401 (2021).

[30] A. Ptok, A. Kobiałka, M. Sternik, J. Łażewski, P. T. Jochym, A. M. Oleś, and P. Piekarz, Dynamical study of the origin of the charge density wave in av 3 sb 5 (a= k, rb, cs) compounds, Physical Review B **105**, 235134 (2022).

[31] Q. Deng, H. Tan, B. R. Ortiz, S. D. Wilson, B. Yan, and L. Wu, Revealing rotational symmetry breaking charge density wave order in the kagome superconductor (rb, k) v 3 sb 5 by ultrafast pump-probe experiments, Physical Review B **111**, 165134 (2025).

[32] M. Kang, S. Fang, J. Yoo, B. R. Ortiz, Y. M. Oey, J. Choi, S. H. Ryu, J. Kim, C. Jozwiak, A. Bostwick, et al., Charge order landscape and competition with superconductivity in kagome metals, Nature Materials **22**, 186 (2022).

[33] D. Subires, A. Korshunov, A. Said, L. Sánchez, B. R. Ortiz, S. D. Wilson, A. Bosak, and S. Blanco-Canosa, Order-disorder charge density wave instability in the kagome metal (cs, rb) v3sb5, Nature Communications **14**, 1015 (2023).

[34] Y. Hu, X. Wu, B. R. Ortiz, X. Han, N. C. Plumb, S. D. Wilson, A. P. Schnyder, M. Shi, et al., Coexistence of trihexagonal and star-of-david pattern in the charge density wave of the kagome superconductor a v 3 sb 5, Physical Review B **106**, L241106 (2022).

[35] C. Li, X. Wu, H. Liu, C. Polley, Q. Guo, Y. Wang, X. Han, M. Dendzik, M. H. Berntsen, B. Thiagarajan, et al., Coexistence of two intertwined charge density waves in a kagome system, Physical Review Research **4**, 033072 (2022).

[36] D. Azoury, A. von Hoegen, Y. Su, K. H. Oh, T. Holder, H. Tan, B. R. Ortiz, A. Capa Salinas, S. D. Wilson, B. Yan, et al., Direct observation of the collective modes of the charge density wave in the kagome metal csv3sb5, Proceedings of the National Academy of Sciences **120**, e2308588120 (2023).

[37] H. Miao, H. X. Li, W. Meier, A. Huon, H. N. Lee, A. Said, H. Lei, B. Ortiz, S. Wilson, J. Yin, et al., Geometry of the charge density wave in the kagome metal a v 3 sb 5, Physical Review B **104**, 195132 (2021).

[38] N. Ratcliff, L. Hallett, B. R. Ortiz, S. D. Wilson, and J. W. Harter, Coherent phonon spectroscopy and interlayer modulation of charge density wave order in the kagome metal csv 3 sb 5, Physical Review Materials **5**, L111801 (2021).

[39] Q. Xiao, Y. Lin, Q. Li, X. Zheng, S. Francoual, C. Plueckthun, W. Xia, Q. Qiu, S. Zhang, Y. Guo, et al., Coexistence of multiple stacking charge density waves in kagome superconductor csv 3 sb 5, Physical Review Research **5**, L012032 (2023).

[40] Y. Wang, T. Wu, Z. Li, K. Jiang, and J. Hu, Structure of the kagome superconductor csv 3 sb 5 in the charge density wave state, Physical Review B **107**, 184106 (2023).

[41] F. Jin, W. Ren, M. Tan, M. Xie, B. Lu, Z. Zhang, J. Ji, and Q. Zhang, π phase interlayer shift and stacking fault in the kagome superconductor csv 3 sb 5, Physical Review Letters **132**, 066501 (2024).

[42] L. Kautzsch, B. R. Ortiz, K. Mallayya, J. Plumb, G. Pokharel, J. P. Ruff, Z. Islam, E.-A. Kim, R. Seshadri, and S. D. Wilson, Structural evolution of the kagome superconductors a v 3 sb 5 (a= k, rb, and cs) through charge density wave order, Physical Review Materials **7**, 024806 (2023).

[43] M. Alkorta, M. Gutierrez-Amigo, C. Guo, P. J. Moll, M. G. Vergniory, and I. Errea, Symmetry-broken charge-ordered ground state in csv _3 sb _5 kagome metal, arXiv preprint arXiv:2505.19686 (2025).

[44] Q. Stahl, D. Chen, T. Ritschel, C. Shekhar, E. Sadrollahi, M. Rahn, O. Ivashko, M. v. Zimmermann, C. Felser, and J. Geck, Temperature-driven reorganization of electronic order in csv 3 sb 5, Physical Review B **105**, 195136 (2022).

[45] J. Plumb, A. C. Salinas, K. Mallayya, E. Kisiel, F. B. Carneiro, R. Gomez, G. Pokharel, E.-A. Kim, S. Sarker, Z. Islam, et al., Phase-separated charge order and twinning across length scales in csv 3 sb 5, Physical Review Materials **8**, 093601 (2024).

[46] Q. Wu, Z. Wang, Q. Liu, R. Li, S. Xu, Q. Yin, C. Gong, Z. Tu, H. Lei, T. Dong, et al., Simultaneous formation of two-fold rotation symmetry with charge order in the kagome superconductor csv 3 sb 5 by optical polarization rotation measurement, Physical Review B **106**, 205109 (2022).

[47] H. Zhao, H. Li, B. R. Ortiz, S. M. Teicher, T. Park, M. Ye, Z. Wang, L. Balents, S. D. Wilson, and I. Zeljkovic, Cascade of correlated electron states in the kagome superconductor csv3sb5, Nature **599**, 216 (2021).

[48] Q. Chen, D. Chen, W. Schnelle, C. Felser, and B. Gaulin, Charge density wave order and fluctuations above t cdw and below superconducting t c in the kagome metal csv 3 sb 5, Physical Review Letters **129**, 056401 (2022).

[49] Y. Zhong, T. Suzuki, H. Liu, K. Liu, Z. Nie, Y. Shi, S. Meng, B. Lv, H. Ding, T. Kanai, et al., Unveiling van hove singularity modulation and fluctuated charge order in kagome superconductor cs v 3 s b 5 via time-resolved arpes, Physical Review Research **6**, 043328 (2024).

[50] Y. R. Shen, Principles of nonlinear optics (Wiley-Interscience, New York, NY, USA, 1984).

[51] Y. R. Shen and N. Bloembergen, Theory of stimulated brillouin and raman scattering, Physical Review **137**, A1787 (1965).

[52] J. A. Giordmaine and W. Kaiser, Light scattering by coherently driven lattice vibrations, Physical Review **144**, 676 (1966).

[53] Z. X. Wang, Q. Wu, Q. W. Yin, C. S. Gong, Z. J. Tu, T. Lin, Q. M. Liu, L. Y. Shi, S. J. Zhang, D. Wu, H. C. Lei, T. Dong, and N. L. Wang, Unconventional charge density wave and photoinduced lattice symmetry change in the kagome metal csv_3sb_5 probed by time-resolved spectroscopy, Phys. Rev. B **104**, 165110 (2021).

[54] E. Uykur, B. Ortiz, O. Iakutkina, M. Wenzel, S. Wilson, M. Dressel, and A. Tsirlin, Low-energy optical properties of the nonmagnetic kagome metal csv 3 sb 5, Physical Review B **104**, 045130 (2021).

[55] J. Joshi, H. M. Hill, S. Chowdhury, C. D. Malliakas, F. Tavazza, U. Chatterjee, A. R. Hight Walker, and P. M. Vora, Short-range charge density wave order in 2 h-t a s 2, Physical Review B **99**, 245144 (2019).

[56] G. Liu, X. Ma, K. He, Q. Li, H. Tan, Y. Liu, J. Xu, W. Tang, K. Watanabe, T. Taniguchi, et al., Observa-

tion of anomalous amplitude modes in the kagome metal csv3sb5, Nature communications **13**, 3461 (2022).
[57] G. He, L. Peis, E. F. Cuddy, Z. Zhao, D. Li, Y. Zhang, R. Stumberger, B. Moritz, H. Yang, H. Gao, et al., Anharmonic strong-coupling effects at the origin of the charge density wave in csv3sb5, Nature Communications **15**, 1895 (2024).
[58] L. Stojchevska, T. Mertelj, J.-H. Chu, I. R. Fisher, and D. Mihailovic, Doping dependence of femtosecond quasiparticle relaxation dynamics in ba (fe, co) 2 as 2 single crystals: Evidence for normal-state nematic fluctuations, Physical Review B **86**, 024519 (2012).
[59] E. Thewalt, I. M. Hayes, J. P. Hinton, A. Little, S. Patankar, L. Wu, T. Helm, C. V. Stan, N. Tamura, J. G. Analytis, et al., Imaging anomalous nematic order and strain in optimally doped bafe 2 (as, p) 2, Physical review letters **121**, 027001 (2018).
[60] S. Liu, C. Zhang, Q. Deng, H.-h. Wen, J.-x. Li, E. E. Chia, X. Wang, and M. Xiao, Transient electronic anisotropy in overdoped naf e 1- x c ox as superconductors, Physical Review B **97**, 020505 (2018).
[61] L. Liu, Y. Li, H. Tan, Y. Liu, Y. Shi, Y. Zhai, H. Lin, G. Cao, B. Yan, G.-M. Zhang, et al., Charge density wave coexisting with amplified nematicity in the correlated kagome metal cscr3sb5, arXiv preprint arXiv:2411.06778 (2024).
[62] R. Merlin, Generating coherent thz phonons with light pulses, Solid state communications **102**, 207 (1997).
[63] T. Stevens, J. Kuhl, and R. Merlin, Coherent phonon generation and the two stimulated raman tensors, Physical Review B **65**, 144304 (2002).
[64] L. Dhar, J. A. Rogers, and K. A. Nelson, Time-resolved vibrational spectroscopy in the impulsive limit, Chemical Reviews **94**, 157 (1994).
[65] Y.-X. Yan, E. B. Gamble Jr, and K. A. Nelson, Impulsive stimulated scattering: General importance in femtosecond laser pulse interactions with matter, and spectroscopic applications, The Journal of chemical physics **83**, 5391 (1985).
[66] I. Gray, Q. Deng, Q. Tian, M. Chilcote, J. S. Dodge, M. Brahlek, and L. Wu, Time-resolved magneto-optical effects in the altermagnet candidate mnte, Applied Physics Letters **125** (2024).
[67] T. Cheng, J. Vidal, H. Zeiger, G. Dresselhaus, M. Dresselhaus, and E. Ippen, Mechanism for displacive excitation of coherent phonons in sb, bi, te, and ti2o3, Applied Physics Letters **59**, 1923 (1991).
[68] H. Zeiger, J. Vidal, T. Cheng, E. Ippen, G. Dresselhaus, and M. Dresselhaus, Theory for displacive excitation of coherent phonons, Physical Review B **45**, 768 (1992).
[69] S. De Silvestri, J. Fujimoto, E. Ippen, E. B. Gamble Jr, L. R. Williams, and K. A. Nelson, Femtosecond time-resolved measurements of optic phonon dephasing by impulsive stimulated raman scattering in α-perylene crystal from 20 to 300 k, Chemical physics letters **116**, 146 (1985).
[70] S. Ruhman, A. G. Joly, and K. A. Nelson, Time-resolved observations of coherent molecular vibrational motion and the general occurrence of impulsive stimulated scattering, The Journal of chemical physics **86**, 6563 (1987).
[71] S. Wu, B. R. Ortiz, H. Tan, S. D. Wilson, B. Yan, T. Birol, and G. Blumberg, Charge density wave order in the kagome metal a v 3 sb 5 (a= cs, rb, k), Physical Review B **105**, 155106 (2022).
[72] K. Nakayama, Y. Li, T. Kato, M. Liu, Z. Wang, T. Takahashi, Y. Yao, and T. Sato, Multiple energy scales and anisotropic energy gap in the charge-density-wave phase of the kagome superconductor csv 3 sb 5, Physical Review B **104**, L161112 (2021).
[73] X. Zhou, Y. Li, X. Fan, J. Hao, Y. Dai, Z. Wang, Y. Yao, and H.-H. Wen, Origin of charge density wave in the kagome metal csv 3 sb 5 as revealed by optical spectroscopy, Physical Review B **104**, L041101 (2021).
[74] Z. Wang, S. Ma, Y. Zhang, H. Yang, Z. Zhao, Y. Ou, Y. Zhu, S. Ni, Z. Lu, H. Chen, et al., Distinctive momentum dependent charge-density-wave gap observed in csv _3 sb _5 superconductor with topological kagome lattice, arXiv preprint arXiv:2104.05556 (2021).
[75] H. Ning, K. H. Oh, Y. Su, A. von Hoegen, Z. Porter, A. Capa Salinas, Q. L. Nguyen, M. Chollet, T. Sato, V. Esposito, et al., Dynamical decoding of the competition between charge density waves in a kagome superconductor, Nature Communications **15**, 7286 (2024).
[76] L. Kautzsch, Y. M. Oey, H. Li, Z. Ren, B. R. Ortiz, G. Pokharel, R. Seshadri, J. Ruff, T. Kongruengkit, J. W. Harter, et al., Incommensurate charge-stripe correlations in the kagome superconductor csv3sb5- x sn x, npj Quantum Materials **8**, 37 (2023).
[77] Z. Wang, Y.-X. Jiang, J.-X. Yin, Y. Li, G.-Y. Wang, H.-L. Huang, S. Shao, J. Liu, P. Zhu, N. Shumiya, et al., Electronic nature of chiral charge order in the kagome superconductor cs v 3 sb 5, Physical Review B **104**, 075148 (2021).
[78] Y. M. Oey, B. R. Ortiz, F. Kaboudvand, J. Frassineti, E. Garcia, R. Cong, S. Sanna, V. F. Mitrović, R. Seshadri, and S. D. Wilson, Fermi level tuning and double-dome superconductivity in the kagome metal csv 3 sb 5- x sn x, Physical Review Materials **6**, L041801 (2022).
[79] Y. Zhong, J. Liu, X. Wu, Z. Guguchia, J.-X. Yin, A. Mine, Y. Li, S. Najafzadeh, D. Das, C. Mielke III, et al., Nodeless electron pairing in csv3sb5-derived kagome superconductors, Nature **617**, 488 (2023).
[80] X. Teng, L. Chen, F. Ye, E. Rosenberg, Z. Liu, J.-X. Yin, Y.-X. Jiang, J. S. Oh, M. Z. Hasan, K. J. Neubauer, et al., Discovery of charge density wave in a kagome lattice antiferromagnet, Nature **609**, 490 (2022).
[81] J. S. Oh, A. Biswas, M. Klemm, H. Tan, M. Hashimoto, D. Lu, B. Yan, P. Dai, R. J. Birgeneau, and M. Yi, Tunability of charge density wave in a magnetic kagome metal, arXiv preprint arXiv:2404.02231 (2024).
[82] G. Kresse and J. Furthmüller, Efficiency of ab-initio total energy calculations for metals and semiconductors using a plane-wave basis set, Computational materials science **6**, 15 (1996).
[83] G. Kresse and J. Furthmüller, Efficient iterative schemes for ab initio total-energy calculations using a plane-wave basis set, Physical review B **54**, 11169 (1996).
[84] J. P. Perdew, K. Burke, and M. Ernzerhof, Generalized gradient approximation made simple, Physical review letters **77**, 3865 (1996).
[85] S. Grimme, J. Antony, S. Ehrlich, and H. Krieg, A consistent and accurate ab initio parametrization of density functional dispersion correction (dft-d) for the 94 elements h-pu, The Journal of chemical physics **132** (2010).
[86] A. Togo and I. Tanaka, First principles phonon calculations in materials science, Scripta Materialia **108**, 1 (2015).

[87] G. A. Garrett, Femtosecond pulsed laser excitation of coherent and squeezed phonon fields (University of Michigan, 2001).

[88] G. Garrett, T. Albrecht, J. Whitaker, and R. Merlin, Coherent thz phonons driven by light pulses and the sb problem: what is the mechanism?, Physical review letters **77**, 3661 (1996).

[89] M. I. Aroyo, J. M. Perez-Mato, C. Capillas, E. Kroumova, S. Ivantchev, G. Madariaga, A. Kirov, and H. Wondratschek, Bilbao crystallographic server: I. databases and crystallographic computing programs, Zeitschrift für Kristallographie-Crystalline Materials **221**, 15 (2006).

[90] M. I. Aroyo, A. Kirov, C. Capillas, J. Perez-Mato, and H. Wondratschek, Bilbao crystallographic server. ii. representations of crystallographic point groups and space groups, Foundations of Crystallography **62**, 115 (2006).

[91] M. I. Aroyo, J. M. Perez-Mato, D. Orobengoa, E. Tasci, G. de la Flor, and A. Kirov, Crystallography online: Bilbao crystallographic server, Bulg. Chem. Commun **43**, 183 (2011).

[92] K. Ishioka, M. Kitajima, and O. V. Misochko, Temperature dependence of coherent a1g and eg phonons of bismuth, Journal of Applied Physics **100** (2006).

APPENDIX A: DFT CALCULATION DETAILS

All density functional theory (DFT) calculations are performed using the Vienna Ab-initio Simulation Package[82, 83]. The exchange–correlation interactions between electrons are treated using the generalized gradient approximation (GGA) of the Perdew–Burke–Ernzerhof (PBE) type[84]. A plane-wave energy cutoff of 300 eV is employed throughout. Structural optimizations with the DFT-D3 method of Grimme with zero-damping function[85] are carried out until the residual forces on all atoms are less than 1 meV/Å. The stable Star-of-David (SD) and inverse Star-of-David (ISD) structures are obtained from previous calculations[29]. For the three-dimensional charge density wave phases, we construct initial structures by stacking the 2D SD and ISD configurations along the c-axis, followed by full structural relaxation. As a result, two energetically favorable phases are identified: an ISD + ISD configuration with an interlayer π-phase shift (point group D_{2h}) and an ISD + SD configuration without a π-phase shift (point group D_{6h}). Phonon dispersions and vibrational modes are calculated using the Phonopy package within the finite-displacement approach[86]. For the D_{2h} structure, a $2 \times 2 \times 2$ supercell is used with a $2 \times 2 \times 2$ k-point mesh for reciprocal space sampling. For the D_{6h} structure, a $2 \times 2 \times 1$ supercell is adopted, along with the same $2 \times 2 \times 2$ k-point mesh.

APPENDIX B: ANISOTROPY SHOWN BY VARYING THE PROBE POLARIZATION BELOW T_{CDW}

We provide here the supplementary data of probe polarization dependence of our TR-reflectivity signal below and above T_{CDW} in CsV_3Sb_5 (Fig. 8).

Clearly, at T = 5 K and 45 K, the TR-reflectivity signal size shows two-fold probe polarization angle dependence. While at T = 100 K, above T_{CDW}, the TR-reflectivity signal size is independent of probe polarization angle. Note for any probe polarization angle φ, $\varphi + 180°$ is equivalent to φ. And for T = 100 K data, only φ = 0 - 180° is shown.

This probe polarization dependent measurements have also been successfully used to probe the breaking of C_6 in Kagome $CsCr_3Sb_5$[61]. $CsCr_3Sb_5$ has space group P6/mmm in the high temperature phase. The authors in [61] also performed TR-reflectivity at various probe polarization directions at different temperatures. Below $T^* = 55$ K, TR-reflectivity shows anisotropy and two-fold dependence on probe polarization directions, while the TRR signals show no probe polarization dependence above T^* in the C_6-preserved high temperature phase. They attribute the anisotropic TR-reflectivity signal at various probe polarization directions to nematicity which breaks C_6 to C_2. From their results, TR-reflectivity signal shows no probe polarization dependence in the C_6-preserved state and shows anisotropic two-fold dependence on probe polarization directions in the C_2 state. Our results are essentially the same as in [61], the only difference is the C_6 breaking in our CsV_3Sb_5 is from the orthorhombic CDW structure induced by interlayer π phase shift which breaks C_6 in the high temperature phase of CsV_3Sb_5 down to C_2.

APPENDIX C: CONFIRMATION OF DECP VIA PUMP POLARIZATION DEPENDENT STUDY

DECP requires absorption at the pump frequency in order to disturb the electronic energy distribution in the material, and only fully symmetric modes can be observed[67, 68] in DECP mechanism. Fully symmetric phonon modes host Γ_1^+ symmetry, such as A_{1g} modes in D_{6h} point group and A_g modes in D_{2h} point group. We acknowledge that there are reports of the observation of non-fully-symmetric coherent phonon modes in literature also in absorbing media, and thus provide a more careful explanation below to confirm all detected modes are fully-symmetric modes.

In the process of impulsive stimulated Raman scattering (ISRS), the amplitude of the coherent phonon is proportional to[87, 88]:

$$\left[E_{pu}^i \left(\frac{\partial \chi^{ij}}{\partial Q}\right)_0 E_{pu}^j\right]\left[E_{pr}^i \left(\frac{\partial \chi^{ij}}{\partial Q}\right)_0 E_{pr}^j\right]$$

where E_{pu} indicates the pump light polarization and E_{pr} indicates the probe polarization. Q is the normal mode amplitude of the phonon, χ is the electric susceptibility, and $\left(\partial\chi^{ij}/\partial Q\right)_0$ is the Raman tensor element. The Raman scattering amplitude is proportional to the square of the modulus of $\left(\partial\chi^{ij}/\partial Q\right)_0$. The Raman tensor form of E_{2g} mode is $\left(\begin{smallmatrix} 0 & -d \\ -d & 0 \end{smallmatrix}\right)$ and $\left(\begin{smallmatrix} d & 0 \\ 0 & -d \end{smallmatrix}\right)$ with only one nonzero independent parameter[89–91].

Above T_{CDW}, previous Raman spectroscopy detected one A_{1g} mode at 4.1 THz and one E_{2g} mode at 3.6 THz with comparable amplitudes[56, 71]. This main 3.6 THz E_{2g} mode persists across T_{CDW} at all temperatures with minimal frequency change of less than 1 cm^{-1} (corresponding to 0.030 THz) and increasing amplitude as temperature increases[56, 71]. However, as seen from Fig. 2b from the main text, in our TR-reflectivity measurements, we only detect the 4.1 THz A_{1g} mode above T_{CDW}. Below T_{CDW}, we do not observe this main 3.6 THz mode either. We do not observe such a mode that matches with the features of Raman-detected 3.6 THz E_{2g} mode, i.e. there is no such a mode near 3.6 THz that persists at all temperatures with increasing amplitude and minimal frequency change (< 0.030 THz) as temperature increases. The closest detected mode is the 3.86 THz mode, but it quickly weakens and softens as temperature increases, in contrast to the 3.6 THz E_{2g} mode. Since the 3.6 THz non-fully symmetric E_{2g} mode has the dominantly maximum Raman scattering amplitude

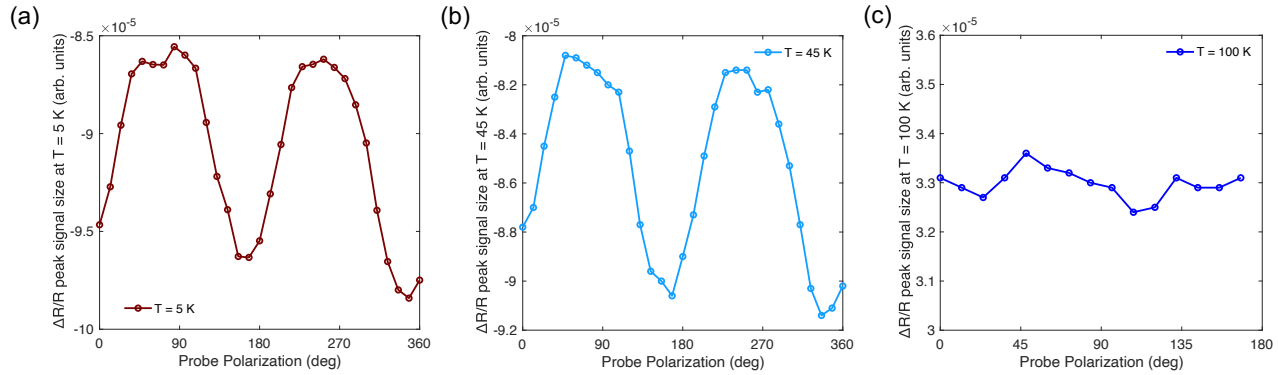

FIG. 8. Probe polarization dependence of ΔR/R peak signal size at T = 5 K, 45 K and 100 K in CsV_3Sb_5. Data is taken at the same spot position as Fig. 5 of the main text.

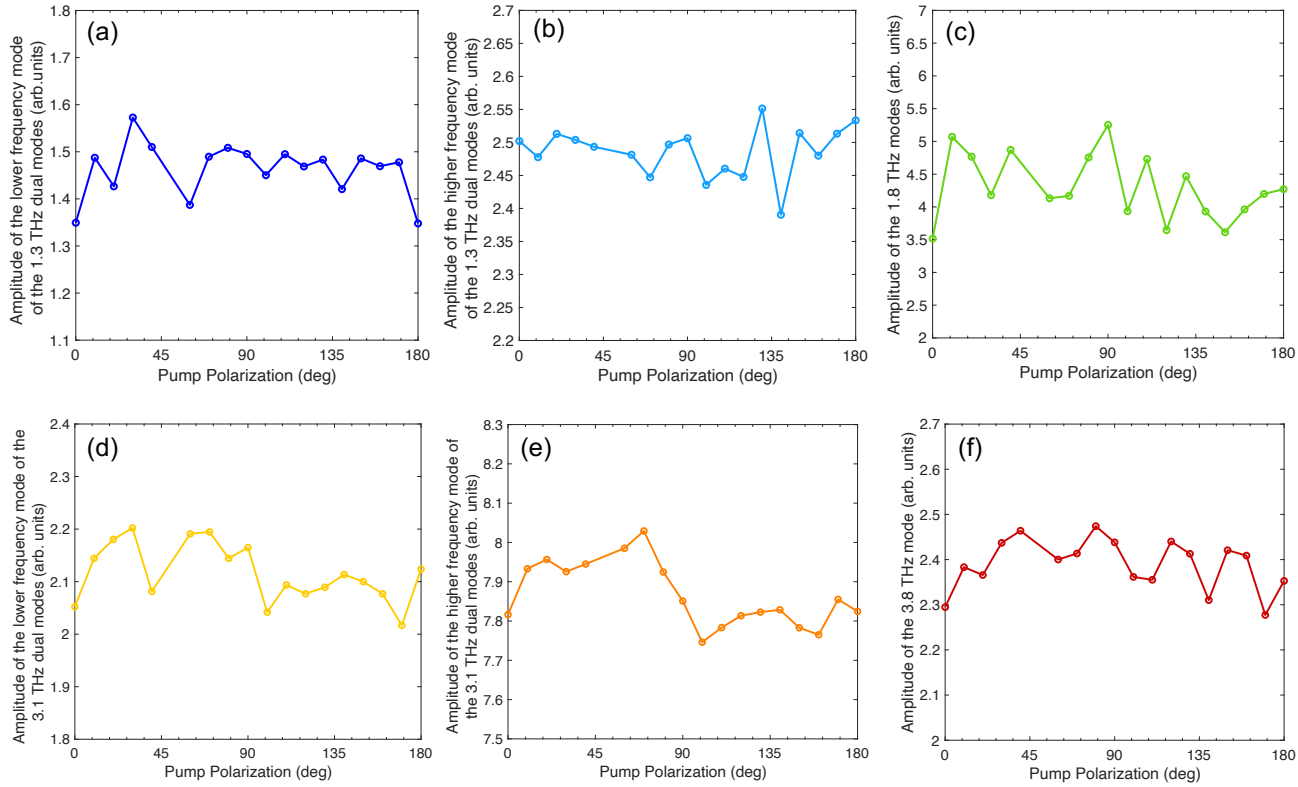

FIG. 9. Pump polarization dependence of the amplitude of coherent phonon modes taken at T = 5 K in CsV_3Sb_5 including the 1.3 THz dual modes, 3.1 THz dual modes, 1.8 THz mode and 3.8 THz mode.

among all non-fully-symmetric Raman-active modes[71], without detecting this mode, we can rule out the detection of non-fully-symmetric Raman modes in our TR-reflectivity measurements.

We also performed additional pump polarization dependent measurements as used in K. Ishioka et al., J. Appl. Phys. 100, 093501 (2006) [92] to determine the symmetry of our observed coherent phonons. Suppose the actual CDW state is C_6-breaking with point group D_{2h}(e.g. ISD + ISD with interlayer π phase shift, SD + ISD with interlayer π phase shift). For non-fully-symmetric Raman modes, when the light is normal incident on (001) surface, one only need to consider B_{1g} mode in D_{2h} point group, with the Raman tensor form of $\left(\begin{smallmatrix} 0 & d \\ d & 0 \end{smallmatrix}\right)$ [89–91]. We denote $E_{pr} = (\cos\theta, \sin\theta)$, where θ is the angle between the probe polarization direction and in-plane axis, and θ is fixed since we fix the probe polarization direction. We denote $E_{pu} = (\cos\varphi, \sin\varphi)$ where φ is the angle of pump polarization direction with respect to in-plane axis. By varying pump polarization

direction, φ is varied. If we consider excitation of non-fully-symmetric Raman active phonons via ISRS, using the above equation, one gets the amplitude of B_{1g} mode via ISRS is: $I_{B_{1g}} \propto \sin 2\varphi$ showing two-fold dependence on pump polarization direction. Here we fix the probe polarization direction and measure the coherent phonon amplitude vs pump polarization direction of our observed 1.3 THz dual modes, 1.8 THz mode, 3.1 THz dual modes, and 3.8 THz mode in the CDW phase, as shown in Fig. 9. The 4.1 THz mode that shows up at all temperature is determined to be the main lattice A_{1g} mode that is present in the high temperature P6/mmm phase. The pump polarization direction is varied between 0 and 180° and we note pump polarization direction between 180° and 360° should be equivalent.

For these observed modes, if they were B_{1g} modes generated via ISRS, $I_{B_{1g}} \propto \sin 2\varphi$, their amplitude should show obvious two-fold dependence on pump polarization direction with nodes where the amplitude goes to zero. However, no observed coherent phonon modes obey this pump polarization dependence. We thus confirm these observed coherent phonon modes are not B_{1g} modes, and they can only be fully-symmetric A_g modes since the pump and probe light are normal incident on (001) surface.

Or, if the actual CDW structure has D_{6h} point group (e.g. $2 \times 2 \times 1$ SD, $2 \times 2 \times 1$ ISD, and SD + ISD without interlayer π phase shift), for non-fully-symmetric Raman-active modes, when the light is normal incident on (001) surface, one will only need to consider E_{2g} mode. Plugging in the Raman tensor of E_{2g} mode gives the amplitude of E_{2g} mode via ISRS as $I_{E_{2g}} \propto \cos 2\varphi$ or $I_{E_{2g}} \propto \sin 2\varphi$. Similarly, the pump polarization dependence of the amplitude of these observed coherent phonon modes does not match with E_{2g} mode, thus the observed coherent phonons can only be fully-symmetric A_{1g} modes. No matter which symmetry we assign to the CDW state, we confirm the observed coherent phonons in the CDW state are fully symmetric. Since all the coherent phonons generated are fully-symmetric mode, our results thus match better with DECP mechanism, same as previous pump-probe studies on CsV_3Sb_5[38].

APPENDIX D: PUMP FLUENCE DEPENDENCE OF COHERENT PHONON SPECTRUM

Here, we also show the coherent phonon spectrum of CsV_3Sb_5 at T = 5 K with varying pump fluence F, up to the maximum pump fluence of 150 μJ/cm^2 of our laser (Fig. 10). All coherent phonon spectra are normalized by the amplitude of the higher frequency mode of the 1.3 THz dual modes. At the lowest pump fluence, we reproduce the 1.3 THz dual modes, 1.8 THz mode, 3.1 THz modes, 3.8 THz mode and 4.1 THz mode reported in our main text, with the 3.1 THz mode having the strongest amplitude. As pump fluence is increased, the 3.1 THz, 3.8 THz and 4.1 THz modes become relatively

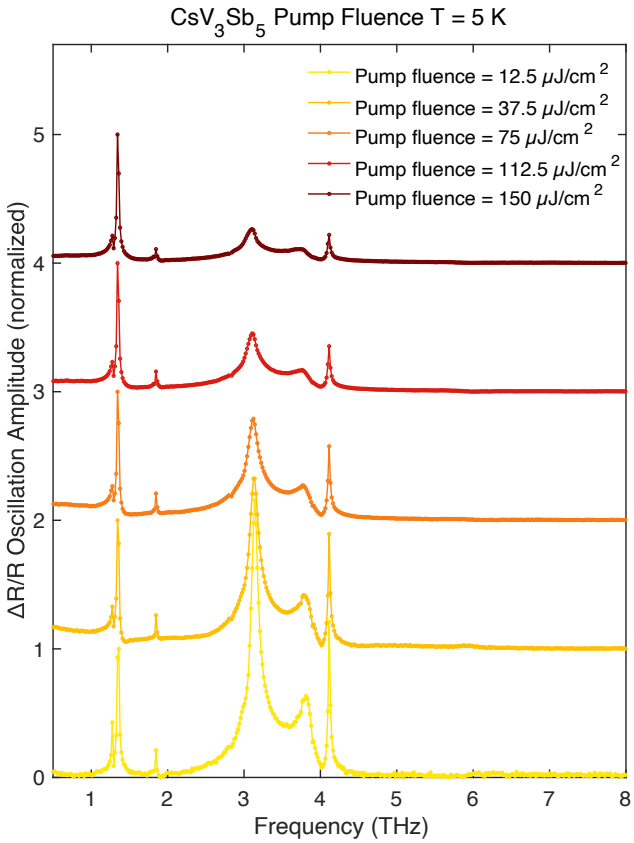

FIG. 10. Pump fluence dependence of the coherent phonon spectrum taken at T = 5 K in CsV_3Sb_5. All datasets are normalized by the higher frequency peak of the 1.3 THz dual modes.

weaker and the higher frequency mode of the 1.3 THz dual modes dominates at high pump fluences.

We also notice the change of the amplitude ratio between the lower frequency and higher frequency mode of the 1.3 THz dual modes as a function of pump fluence. From Fig. 10, one can find the lower frequency peak of the 1.3 THz dual modes becomes relatively weaker with respect to the higher frequency peak of the 1.3 THz dual modes as the pump fluence increases. For these two peaks of the 1.3 THz dual modes, we plot the ratio of the lower frequency peak amplitude to the higher frequency peak amplitude as a function of pump fluence in Fig. 11a, showing the decrease of this ratio as pump fluence is increased. This indicates the amplitude of the lower frequency peak of the 1.3 THz dual modes gets suppressed with respect to the amplitude of the higher frequency peak of the 1.3 THz dual modes. We rule out the effect of increased laser heating at higher fluences by plotting the temperature dependence of this peak amplitude ratio with fixed pump fluence of $\sim 10\mu$J/cm^2 (Fig. 11b). This peak amplitude ratio does not show monotonic decrease as temperature increases, and its value stays near 0.4, compared to ~ 0.15 at high fluences.

In DECP mechanism, the coherent phonon amplitude

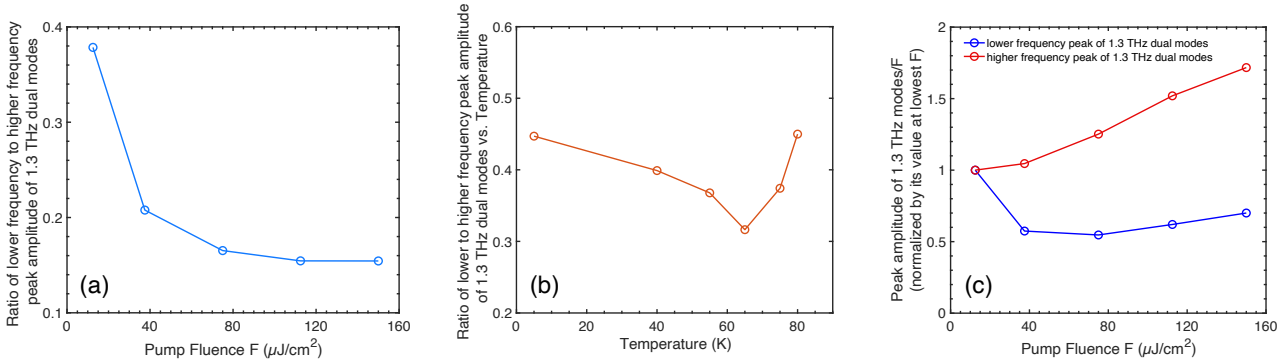

FIG. 11. **Peak amplitudes of 1.3 THz dual modes as pump fluence changes.** (a) The ratio of lower frequency to higher frequency peak amplitude of 1.3 THz dual modes vs. pump fluence. Data extracted from Fig. 10. (b) The ratio of lower frequency to higher frequency peak amplitude of 1.3 THz dual modes vs. temperature. (c) Peak amplitude of 1.3 THz modes/F (normalized by its value at lowest F) as a function of pump fluence. Data extracted from Fig. 10.

in $\Delta R/R$ is proportional to pump fluence[68]. Thus, for an independent coherent phonon, its amplitude normalized by pump fluence will be a constant. In Fig. 11c, we show the peak amplitude divided by pump fluence of the lower and higher frequency peak of the 1.3 THz dual modes as a function of pump fluence. Note we normalize each curve by its value at lowest pump fluence to better compare these two curves. The peak amplitude/pump fluence of the higher frequency peak shows increasing behavior, but the peak amplitude/pump fluence of the lower frequency peak got suppressed. The opposite trend of these two peaks suggests a competition behavior between them.

These observations match with a recent TR-XRD study demonstrating the coexistence of MLL and LLL phases and competition between these two coexisting CDW phases in CsV_3Sb_5[75]. Herein, upon light excitation, the LLL phase gets more suppressed with respect to MLL, along with an expansion of the MLL domain and a contraction of the LLL domain. Thus, the lower frequency peak of the 1.3 THz dual modes will come from the more suppressed LLL phase and the higher frequency peak of the 1.3 THz dual modes will come from MLL phase. Indeed, as seen from the calculated fully-symmetric phonon spectrum of the coexistence of MLL and LLL state in Fig. 6c and Table I of the main text, we can indeed find a 1.04 THz fully-symmetric mode from LLL and a 1.21 THz fully-symmetric mode from MLL that can match with our detected 1.3 THz dual modes in TR-reflectivity. Thus, this picture with the coexistence of MLL and LLL CDW phase matches with our TR-reflectivity results, and the fluence dependent ultrafast TR-reflectivity study reveals the competition of these two CDW phases. Our non-equilibrium dynamical study of this system thus provides more details of the exact CDW configuration and decodes the interplay between coexisting CDW phases.